Available online at www.sciencedirect.com
ScienceDirect
Journal of Computational Physics 227 (2008) 4805–4824
JOURNAL OF COMPUTATIONAL PHYSICS
www.elsevier.com/locate/jcp

A stable high-order finite difference scheme for the compressible Navier–Stokes equations No-slip wall boundary conditions

Magnus Svärd [a,*], Jan Nordström [b,c,d]

[a] Centre of Mathematics for Applications, University of Oslo, P.O. Box 1053, Blindern, N-0316 Oslo, Norway
[b] Department of Computational Physics, The Swedish Defense Research Agency, SE-164 90 Stockholm, Sweden
[c] Department of Information Technology, Uppsala University, SE-751 05 Uppsala, Sweden
[d] Department of Aeronautical and Vehicle Engineering, KTH—The Royal Institute of Technology, SE-100 44 Stockholm, Sweden

Received 5 June 2007; received in revised form 18 December 2007; accepted 18 December 2007
Available online 2 February 2008

Abstract

A stable wall boundary procedure is derived for the discretized compressible Navier–Stokes equations. The procedure leads to an energy estimate for the linearized equations. We discretize the equations using high-order accurate finite difference summation-by-parts (SBP) operators. The boundary conditions are imposed weakly with penalty terms. We prove linear stability for the scheme including the wall boundary conditions.

The penalty imposition of the boundary conditions is tested for the flow around a circular cylinder at $Ma = 0.1$ and $Re = 100$. We demonstrate the robustness of the SBP-SAT technique by imposing incompatible initial data and show the behavior of the boundary condition implementation. Using the errors at the wall we show that higher convergence rates are obtained for the high-order schemes.

We compute the vortex shedding from a circular cylinder and obtain good agreement with previously published (computational and experimental) results for lift, drag and the Strouhal number. We use our results to compare the computational time for a given for a accuracy and show the superior efficiency of the 5th-order scheme.

1. Introduction

The no-slip wall boundary condition is numerically difficult to implement in a stable and accurate manner. Moreover, one frequently has to face the difficulty with incompatible initial data. Realistic computations are often initialized with constant free-stream values in the entire domain, which obviously does not satisfy a no-slip boundary condition. This causes large oscillations and possible blow-ups. The problem can, to some extent, be circumvented by constructing initial data that satisfy the boundary conditions, but that is a tedious

* Corresponding author.
E-mail addresses: magnus.svard@gmail.com (M. Svärd), jan.nordstrom@foi.se (J. Nordström).

0021-9991/$ - see front matter © 2008 Elsevier Inc. All rights reserved.
doi:10.1016/j.jcp.2007.12.028

task. The aim of this article is to demonstrate a technique that easily handles the wall boundary conditions for finite difference methods with orders ranging from 2 to 5.

We approach this problem by deriving a set of (well-known and) well-posed wall boundary conditions for the continuous problem. The Navier–Stokes equations are discretized with high-order finite difference schemes, satisfying a summation-by-parts (SBP) rule. The main contribution of this article is the weak implementation of the boundary conditions with a penalty technique known as simultaneous approximation term (SAT). (For SBP-SAT theory see [9,10,22,2,3,14,15,11,12,23,13,20,21,19].) We prove the scheme stable, including the wall boundary conditions, using the energy method.

In this article we focus on wall boundary conditions. We use the stable treatment of far-field boundaries derived in [19], and in a future article we will discuss a grid–block interface treatment. We merely assume that grid–block interfaces can be treated in a stable manner. With that assumption, the entire scheme is provably stable. In [13], stable artificial dissipation operators were derived, compatible with the SBP-SAT schemes, which are also used. No other features are necessary.

1.1. Advection–diffusion equation

To introduce the idea of the penalty imposition of wall boundary conditions, we will study the advection–diffusion equation

$$\begin{aligned} &u_t + au_x = \epsilon u_{xx}, \quad 0 \leqslant x \leqslant 1, t \geqslant 0, \\ &u(0,t) = 0, \quad au(1,t) - 2\epsilon u_x(1,t) = 0, \quad u(x,0) = f(x), \end{aligned} \tag{1}$$

where $a, \epsilon > 0$. The boundary at $x = 0$ is a model of the wall (and the boundary $x = 1$ mimics a far-field boundary condition). Apply the energy method

$$\frac{1}{2}\left(\int_0^1 u^2\,\mathrm{d}x\right)_t + \frac{au^2}{2}|_0^1 = \epsilon u u_x|_0^1 - \epsilon\int_0^1 u_x^2\,\mathrm{d}x.$$

Using the boundary conditions yields

$$\frac{1}{2}\left(\int_0^1 u^2\,\mathrm{d}x\right)_t + \epsilon\int_0^1 u_x^2\,\mathrm{d}x = 0.$$

Hence, $\|u\|$ is bounded and (1) is well-posed.

1.2. Summation-by-parts

Discretize $0 \leqslant x \leqslant 1$ using $N+1$ evenly distributed grid points with spacing h. Let $v(t) = (v_0(t), \ldots, v_N(t))^{\mathrm{T}}$ be a scalar grid function. Then the first derivative is approximated by, $P^{-1}Qv$, where P is a positive definite (symmetric) matrix. P is used to define a discrete an l_2-equivalent norm, $\|v\|_P^2 = v^{\mathrm{T}}Pv$. In our particular schemes P is diagonal, which is a necessary requirement for stability on curvilinear grids. (See [23].) Q skew-symmetric except at the corners and $Q + Q^{\mathrm{T}} = \mathrm{diag}(-1, 0, \ldots, 0, 1) = B$. Also, let $E_0 = \mathrm{diag}(1, 0, \ldots, 0)$ and $E_1 = \mathrm{diag}(0, \ldots, 0, 1)$.

1.3. Semidiscrete advection–diffusion equation

We discretize (1) as follows

$$v_t + aP^{-1}Qv = \epsilon P^{-1}QP^{-1}Qv + \sigma_L E_0 P^{-1}(v - g_L) + \sigma_R E_1 P^{-1}(av - 2\epsilon P^{-1}Qv - g_R),$$

where σ_L and σ_R are parameters to be determined with respect to stability. With $g_L = g_R = 0$, we apply the energy method by multiplying by $v^{\mathrm{T}}P$ and adding the result to its transpose

$$(\|v\|_P^2)_t + av^{\mathrm{T}}Bv = 2\epsilon v^{\mathrm{T}}BP^{-1}Qv - 2\epsilon(P^{-1}Qv)^{\mathrm{T}}P(P^{-1}Qv) + 2\sigma_L v^{\mathrm{T}}E_0 v + 2\sigma_R v^{\mathrm{T}}E_1(av - 2\epsilon P^{-1}Qv). \tag{2}$$

With $\sigma_R = 1/2$, all boundary terms at $x = 1$ cancel and the right boundary is stable. (See [19] for more details.) We will use the short-hand notation $v_{xi} = (P^{-1}Qv)_i$ and assume that P is diagonal with the upper-left component hp_0. (Note that $p_0 > 0$.) Then

$$(\|v\|_P^2)_t - av_0^2 = -2\epsilon v_0 v_{x0} - 2\epsilon v_x^{\mathrm{T}} P v_x + 2\sigma_L v_0^2. \tag{3}$$

The aim is to choose σ_L such that $\|v\|$ becomes non-increasing. ($\|v\|$ should not increase since the boundary data is 0.) To achieve that, we would like to rewrite the boundary terms as a quadratic form. Since no boundary term with v_{x0}^2 appears explicitly, it seems to be an impossible task. However, we may use

$$v_x^{\mathrm{T}} P v_x = v_{x0}^2 hp_0 + h\sum_{i=1}^{N} v_{xi}^2 p_i = v_{x0}^2 hp_0 + \|v_x\|_{\mathcal{P}}^2. \tag{4}$$

Then (3) becomes

$$(\|v\|_P^2)_t + 2\epsilon\|v_x\|_{\mathcal{P}}^2 + q^{\mathrm{T}} M q = 0,$$

where $q^{\mathrm{T}} = (v_0, v_{x0})$ and

$$M = \begin{pmatrix} -2\sigma_L - a & \epsilon \\ \epsilon & 2\epsilon hp_0 \end{pmatrix}.$$

If M is positive semidefinite, the scheme is stable. Introduce, $\sigma_L = \sigma_1 + \epsilon\sigma_2$ and split M such that

$$M = M_1 + \epsilon M_2 = \begin{pmatrix} -2\sigma_1 - a & 0 \\ 0 & 0 \end{pmatrix} + \epsilon \begin{pmatrix} -2\sigma_2 & 1 \\ 1 & 2hp_0 \end{pmatrix}.$$

M is positive semidefinite, if M_1 and M_2 are. M_1 is positive semidefinite if $\sigma_1 \leqslant -a/2$ and M_2 if $\sigma_2 \leqslant -\frac{1}{4hp_0}$. The same idea will be used for the Navier–Stokes equations, although the algebra will be more complicated.

2. The Navier–Stokes equations

For the benefit of the reader, we summarize the equations and notation introduced in [19], where more details can be found. A bar denotes a dimensional variable, a $*$ a nondimensional variable and ∞ signifies a free-stream value. We nondimensionalize the velocity components $\bar{u}_1, \bar{u}_2, \bar{u}_3$ using the speed of sound $\bar{a}_\infty$; the density $\rho^* = \bar{\rho}/\bar{\rho}_\infty$; the temperature $T^* = \overline{T}/\overline{T}_\infty$; the pressure $p^* = \bar{p}/(\bar{\rho}_\infty \bar{a}_\infty^2)$ and the total energy $e^* = \bar{e}/(\bar{\rho}_\infty \bar{a}_\infty^2)$. λ and μ are the second and shear viscosity coefficients nondimensionalized by $\bar{\mu}_\infty$. We assume that $3\lambda + 2\mu \geqslant 0$ (and in computations and use $\lambda = -2\mu/3$). q^* denotes the heat flux and γ is the ratio of the specific heats. Further, $Re = \frac{u_\infty \rho_\infty L}{\mu_\infty}$, $Ma = \frac{u_\infty}{a_\infty} = u_\infty$, $Pr = \frac{\mu_\infty c_p}{\kappa_\infty}$, are the Reynolds number, Mach number and Prandtl number, where u_∞ denotes the magnitude of the free-stream velocity. We introduce $\epsilon = Ma/Re$ and present the governing equations in nondimensional form on a general domain.

Introduce the coordinate transformation $x = x(\xi, \eta, \zeta)$, $y = y(\xi, \eta, \zeta)$ and $z = z(\xi, \eta, \zeta)$ such that $0 \leqslant \xi, \eta, \zeta \leqslant 1$ (which is the computational domain D) and define the Jacobian matrix as

$$\mathbf{J} = \begin{pmatrix} \frac{\partial x}{\partial \xi} & \frac{\partial x}{\partial \eta} & \frac{\partial x}{\partial \zeta} \\ \frac{\partial y}{\partial \xi} & \frac{\partial y}{\partial \eta} & \frac{\partial y}{\partial \zeta} \\ \frac{\partial z}{\partial \xi} & \frac{\partial z}{\partial \eta} & \frac{\partial z}{\partial \zeta} \end{pmatrix}.$$

Let $\det(\mathbf{J}) = J$, then the Navier–Stokes equations can then be stated on conservative form as

$$(Ju)_t + \widehat{F}_\xi + \widehat{G}_\eta + \widehat{H}_\zeta = 0, \tag{5}$$

where $\widehat{F} = \widehat{F}^{\mathrm{I}} - \epsilon\widehat{F}^{\mathrm{V}}$, $\widehat{G} = \widehat{G}^{\mathrm{I}} - \epsilon\widehat{G}^{\mathrm{V}}$, $\widehat{H} = \widehat{H}^{\mathrm{I}} - \epsilon\widehat{H}^{\mathrm{V}}$. Furthermore

$$\begin{aligned} \widehat{F}^{\mathrm{I,V}} &= J(\xi_x F^{\mathrm{I,V}} + \xi_y G^{\mathrm{I,V}} + \xi_z H^{\mathrm{I,V}}), \\ \widehat{G}^{\mathrm{I,V}} &= J(\eta_x F^{\mathrm{I,V}} + \eta_y G^{\mathrm{I,V}} + \eta_z H^{\mathrm{I,V}}), \\ \widehat{H}^{\mathrm{I,V}} &= J(\zeta_x F^{\mathrm{I,V}} + \zeta_y G^{\mathrm{I,V}} + \zeta_z H^{\mathrm{I,V}}). \end{aligned} \tag{6}$$

A superscript I denotes the inviscid part of the flux and V the viscous part. For a thorough derivation of the transformed Navier–Stokes equations see [16,19].

To analyze these equations in terms of well-posedness we need a set of symmetric linear equations [7,4]. We transform the Navier–Stokes equations to primitive variables $v = (\rho^*, u_1^*, u_2^*, u_3^*, p^*)$, linearize and freeze the coefficients. A tilde sign will denote the time-dependent variable. Variables and matrices without the tilde are their frozen equivalents.

Remark. Formally, we let $\rho^* = \rho_{ex} + \tilde{\rho}$ where ρ_{ex} is the exact (and assumed smooth) solution. We freeze ρ_{ex}, denoted ρ. If we can show well-posedness (or stability in the discrete case) for all ρ in the range of ρ_{ex} the nonlinear problem is well-posed (or stable). (See [7,4] and references therein.)

Next, we use the symmetrizing matrices (S_P, S_p^{-1}), derived in [1], and apply the coordinate transformation described above, to arrive at

$$(J\tilde{w})_t + (\widehat{F}_w)_\xi + (\widehat{G}_w)_\eta + (\widehat{H}_w)_\zeta = 0, \tag{7}$$

where

$$\begin{aligned}
\widehat{F}_w^{\mathrm{I}} &= J(\xi_x A_{1w} + \xi_y A_{2w} + \xi_z A_{3w})u = \widehat{A}_{1w}\tilde{w},\\
\widehat{G}_w^{\mathrm{I}} &= J(\eta_x A_{1w} + \eta_y A_{2w} + \eta_z A_{3w})u = \widehat{A}_{2w}\tilde{w},\\
\widehat{H}_w^{\mathrm{I}} &= J(\zeta_x A_{1w} + \zeta_y A_{2w} + \zeta_z A_{3w})u = \widehat{A}_{3w}\tilde{w}
\end{aligned}$$

and

$$\begin{aligned}
\widehat{F}_w^{\mathrm{V}} &= (\widehat{B}_{11}u_\xi) + (\widehat{B}_{12}u_\eta) + (\widehat{B}_{13}u_\zeta),\\
\widehat{G}_w^{\mathrm{V}} &= (\widehat{B}_{21}u_\xi) + (\widehat{B}_{22}u_\eta) + (\widehat{B}_{33}u_\zeta),\\
\widehat{H}_w^{\mathrm{V}} &= (\widehat{B}_{31}u_\xi) + (\widehat{B}_{32}u_\eta) + (\widehat{B}_{33}u_\zeta),
\end{aligned} \tag{8}$$

where $\widehat{B}_{ij}$ includes the coordinate transformations and their exact forms can be found in [16].

Throughout this paper, u will denote the conservative variables; v the primitive; $\tilde{w}$ the symmetrized (after linearization) and $\tilde{c}$ the characteristic (also after linearization). Using the linearized equation of state, $\tilde{w}$ can be cast as

$$\tilde{w} = \left(\frac{a}{\sqrt{\gamma}\rho}\tilde{\rho}, \tilde{u}_1, \tilde{u}_2, \tilde{u}_3, \frac{1}{\sqrt{\gamma}\sqrt{\gamma-1}a}\widetilde{T}\right). \tag{9}$$

2.1. Well-posedness

Next, we turn to well-posedness of Eq. (7). Apply the energy method to (7)

$$\begin{aligned}
0 = &\int_D \tilde{w}^{\mathrm{T}}\tilde{w}_t J\,\mathrm{d}\xi\,\mathrm{d}\eta\,\mathrm{d}\zeta + \int_D \tilde{w}^{\mathrm{T}}((\widehat{F}_w^{\mathrm{I}})_\xi + (\widehat{G}_w^{\mathrm{I}})_\eta + (\widehat{H}_w^{\mathrm{I}})_\zeta)\mathrm{d}\xi\,\mathrm{d}\eta\,\mathrm{d}\zeta - \epsilon\int_D \tilde{w}^{\mathrm{T}}((\widehat{F}_w^{\mathrm{V}})_\xi + (\widehat{G}_w^{\mathrm{V}})_\eta\\
&+ (\widehat{H}_w^{\mathrm{V}})_\zeta)\mathrm{d}\xi\,\mathrm{d}\eta\,\mathrm{d}\zeta.
\end{aligned} \tag{10}$$

Integrating (10) by parts leads to

$$\begin{aligned}
2\int_D \tilde{w}^{\mathrm{T}}\tilde{w}_t J\,\mathrm{d}\xi\,\mathrm{d}\eta\,\mathrm{d}\zeta + 2\epsilon DI = &\int_{\xi=0} \tilde{w}^{\mathrm{T}}(\widehat{A}_{1w}\tilde{w} - 2\epsilon\widehat{F}_w^{\mathrm{V}})\mathrm{d}\eta\,\mathrm{d}\zeta + \int_{\xi=1} \tilde{w}^{\mathrm{T}}(-\widehat{A}_{1w}\tilde{w} + 2\epsilon\widehat{F}_w^{\mathrm{V}})\mathrm{d}\eta\,\mathrm{d}\zeta\\
&+ \int_{\eta=0} \tilde{w}^{\mathrm{T}}(\widehat{A}_{2w}\tilde{w} - 2\epsilon\widehat{G}_w^{\mathrm{V}})\mathrm{d}\xi\,\mathrm{d}\zeta + \int_{\eta=1} \tilde{w}^{\mathrm{T}}(-\widehat{A}_{2w}\tilde{w} + 2\epsilon\widehat{G}_w^{\mathrm{V}})\mathrm{d}\xi\,\mathrm{d}\zeta\\
&+ \int_{\zeta=0} \tilde{w}^{\mathrm{T}}(\widehat{A}_{3w}\tilde{w} - 2\epsilon\widehat{H}_w^{\mathrm{V}})\mathrm{d}\xi\,\mathrm{d}\eta + \int_{\zeta=1} \tilde{w}^{\mathrm{T}}(-\widehat{A}_{3w}\tilde{w} + 2\epsilon\widehat{H}_w^{\mathrm{V}})\mathrm{d}\xi\mathrm{d}\eta,
\end{aligned} \tag{11}$$

where DI is a positive quadratic term in the derivatives of $\tilde{w}$ (see [16]).

2.2. Wall boundary conditions

In order to simplify the notation, we will study the case of a wall at $\xi = 0$ and assume that all other boundary terms are well-posed and omit (without restriction) their contributions. Then Eq. (11) reduces to

$$2\int_D \tilde{w}^{\mathrm{T}}\tilde{w}_t J \mathrm{d}\xi\,\mathrm{d}\eta\,\mathrm{d}\zeta + 2\epsilon DI = \int_{\xi=0} \tilde{w}^{\mathrm{T}}(\widehat{A}_{1w}\tilde{w} - 2\epsilon\widehat{F}^{\mathrm{V}}_w)\mathrm{d}\eta\,\mathrm{d}\zeta. \tag{12}$$

The right-hand side of (12) will be supplied with boundary conditions in order to bound the solution. In the case of a wall, maximally four boundary conditions may be imposed (see for example [7]). The so called no-slip boundary conditions are $u_1 = u_2 = u_3 = 0$. The fourth condition is usually the temperature $T = g_1$, or the wall-normal temperature gradient, $\frac{\partial T}{\partial n} = g_2$, where g_1 and g_2 are known and bounded functions. We will now show that these two cases are well-posed. Carrying out the coordinate transformations we obtain

$$\widehat{A}_{1w} = J\xi_x\begin{pmatrix} u_1 & b & 0 & 0 & 0\\ & u_1 & 0 & 0 & d\\ 0 & 0 & u_1 & 0 & 0\\ 0 & 0 & 0 & u_1 & 0\\ 0 & d & 0 & 0 & u_1 \end{pmatrix} + J\xi_y\begin{pmatrix} u_2 & 0 & b & 0 & 0\\ 0 & u_2 & 0 & 0 & 0\\ b & 0 & u_2 & 0 & d\\ 0 & 0 & 0 & u_2 & 0\\ 0 & 0 & d & 0 & u_2 \end{pmatrix} + J\xi_z\begin{pmatrix} u_3 & 0 & 0 & b & 0\\ 0 & u_3 & 0 & 0 & 0\\ 0 & 0 & u_3 & 0 & 0\\ b & 0 & 0 & u_3 & d\\ 0 & 0 & 0 & d & u_3 \end{pmatrix},$$

where $b = a/\sqrt{\gamma}$ and $d = \frac{\sqrt{\gamma-1}}{\gamma}$. Insert the boundary conditions $u_1 = u_2 = u_3 = 0$ to obtain

$$\widehat{A}_{1w} = J\begin{pmatrix} 0 & \xi_x b & \xi_y b & \xi_z b & 0\\ \xi_x b & 0 & 0 & 0 & \xi_x d\\ \xi_y b & 0 & 0 & 0 & \xi_y d\\ \xi_z b & 0 & 0 & 0 & \xi_z d\\ 0 & \xi_x d & \xi_y d & \xi_z d & 0 \end{pmatrix}.$$

Inserting $\tilde{u}_1 = \tilde{u}_2 = \tilde{u}_3 = 0$ in (9), we obtain $\tilde{w}^{\mathrm{T}}A_1\tilde{w} = 0$.

Turning to the viscous terms, we study the Cartesian case and the boundary at $x = 0$ to avoid cumbersome notation. Since the first component of the viscous flux is 0 (even in the symmetrized variables), the viscous terms (in the Cartesian case) reduce to,

$$-2\epsilon\tilde{w}^{\mathrm{T}}\widehat{F}^{\mathrm{V}} = -2\epsilon\frac{\gamma\mu}{Pr\rho}\left(\frac{1}{\sqrt{\gamma}\sqrt{\gamma-1}a}\right)^2\widetilde{T}\widetilde{T}_x.$$

Obviously $\widetilde{T} = 0$ bounds the solution, and so does $\widetilde{T}_x = 0$. The condition $\widetilde{T}_x = 0$ corresponds to specifying the normal derivative, $\frac{\widetilde{\partial T}}{\partial n} = (\xi_x\widetilde{T}_\xi + \eta_x\widetilde{T}_\eta + \zeta_x\widetilde{T}_\zeta)/\sqrt{\xi_x^2+\eta_x^2+\zeta_x^2} = 0$, which leads to well-posedness in the general case. We summarize the results in the the following proposition.

Proposition 2.1. *Eq. (7) with $u_i = \tilde{u}_i = 0$ and, $T = g_1(t)$, $\widetilde{T} = 0$ or $\frac{\partial T}{\partial n} = g_2, \frac{\widetilde{\partial T}}{\partial n} = 0$ is well posed.*

Remark. We do not claim Proposition 2.1 to be a new result but include it for completeness of this exposition.

Remark. Above, we have used the linearized version of the boundary conditions. Formally this is justified by the following argument. The no-slip boundary condition is $u_i^* = 0$, $i = 1,2,3$ or $u_i^* = u_{i,\mathrm{ex}} + \tilde{u}_i = 0$. In this case the exact solution is constant on the boundary and $u_{i,\mathrm{ex}} = u_i = 0$. Hence, $\tilde{u}_i = 0$ as well. A similar argument holds for the temperature.

2.3. Discretization

The SBP-SAT method has successfully been used to prove energy-stable discretizations of far-field boundary conditions in [14] and recently in [19] generalized to the three-dimensional equations. The definition of

SBP operators was introduced in Section 1.2 and a compact tensor notation that simplifies the description of the discrete Navier–Stokes equations was introduced in [19]. We will briefly explain the notation.

Let the discrete solution field be u^{ijkl} where the indices represent ξ, η and ζ positions and variable. The three first are spatial indices ranging between, $0 \cdots n_\xi$, $0 \cdots n_\eta$ and $0 \cdots n_\zeta$. The last index ranges between 1 and 5 and represents the five different variables. Order a vector $\mathbf{u} = (u^{0001}, u^{1001}, \ldots, u^{n_\xi, n_\eta, n_\zeta, 5})^{\mathrm{T}}$. We introduce tensor operators based on the following generic rule (stated for the arbitrary 1-D operators $O_{\xi,\eta,\zeta}$)

$$\mathbf{O}_\xi = (I_\zeta \otimes I_\eta \otimes O_\xi \otimes I_5), \quad \mathbf{O}_\eta = (I_\zeta \otimes O_\eta \otimes I_\xi \otimes I_5),$$
$$\mathbf{O}_\zeta = (O_\zeta \otimes I_\eta \otimes I_\xi \otimes I_5),$$

where I_5 denotes a 5×5-identity matrix and $\otimes$ is the Kronecker product. Further

$$\mathbf{P}_{\xi\eta} = \mathbf{P}_\xi \mathbf{P}_\eta, \quad \mathbf{P}_{\eta\zeta} = \mathbf{P}_\eta \mathbf{P}_\zeta,$$
$$\mathbf{P}_{\xi\zeta} = \mathbf{P}_\xi \mathbf{P}_\zeta, \quad \mathbf{P} = \mathbf{P}_\xi \mathbf{P}_\eta \mathbf{P}_\zeta$$

and $\mathbf{E}_{0\xi} = (I_\zeta \otimes I_\eta \otimes E_0 \otimes I_5)$ and $\mathbf{E}_{1\xi}, \mathbf{E}_{0,\eta}$, etc., are defined similarly. We define the norm $\mathbf{u}^{\mathbf{T}}\mathbf{P}\mathbf{u} = \|\mathbf{u}\|^2$. Finally, we will need $\mathbf{A}_{\mathbf{iw}} = (I_\zeta \otimes I_\eta \otimes I_\xi \otimes A_{iw})$.

2.4. Stability of the Navier–Stokes equations

With the same ordering as $\mathbf{u}(t)$, we define the contravariant inviscid fluxes vectors, $\widehat{\mathbf{F}}^{\mathbf{I}}, \widehat{\mathbf{G}}^{\mathbf{I}}, \widehat{\mathbf{H}}^{\mathbf{I}}$ and the viscous flux vectors $\widehat{\mathbf{F}}^{\mathbf{V}}, \widehat{\mathbf{G}}^{\mathbf{V}}, \widehat{\mathbf{H}}^{\mathbf{V}}$ with components $F^{\mathbf{I},ijkl}$, etc. Finally, $(\mathbf{Ju})^{ijkl} = J(\xi_j, \eta_k, \zeta_l)u^{ijkl}$. Note that J is positive for all j, k, l, since we require a coordinate transformation to be non-singular everywhere (i.e. no cell collapses to 0 volume). We use the convention that a colon instead of an index means the vector formed by that index. For instance, $u^{ijk:} = (u^{ijk1}, \ldots, u^{ijk5})$.

Without introducing the penalty terms for the boundary conditions yet, the non-linear Navier–Stokes equations are discretized as

$$(\mathbf{Ju})_t + \mathbf{D}_\xi(\widehat{\mathbf{F}}^{\mathbf{I}} - \epsilon\widehat{\mathbf{F}}^{\mathbf{V}}) + \mathbf{D}_\eta(\widehat{\mathbf{G}}^{\mathbf{I}} - \epsilon\widehat{\mathbf{G}}^{\mathbf{V}}) + \mathbf{D}_\zeta(\widehat{\mathbf{H}}^{\mathbf{I}} - \epsilon\widehat{\mathbf{H}}^{\mathbf{V}}) = \mathbf{0}. \tag{13}$$

As in the continuous case we transform to primitive variables, freeze the coefficients and apply the symmetrizing matrices to obtain

$$(\mathbf{Jw})_t + \mathbf{D}_\xi(\widehat{\mathbf{F}}^{\mathbf{I}}_{\mathbf{w}} - \epsilon\widehat{\mathbf{F}}^{\mathbf{V}}_{\mathbf{w}}) + \mathbf{D}_\eta(\widehat{\mathbf{G}}^{\mathbf{I}}_{\mathbf{w}} - \epsilon\widehat{\mathbf{G}}^{\mathbf{V}}_{\mathbf{w}}) + \mathbf{D}_\zeta(\widehat{\mathbf{H}}^{\mathbf{I}}_{\mathbf{w}} - \epsilon\widehat{\mathbf{H}}^{\mathbf{V}}_{\mathbf{w}}) = \mathbf{0}, \tag{14}$$

where the viscous fluxes the discrete equivalents to (8). The derivatives appearing in the viscous fluxes are computed with $\mathbf{D}_\xi$, $\mathbf{D}_\eta$ and $\mathbf{D}_\zeta$. We now apply the energy method to (14) and obtain

$$\|\sqrt{\mathbf{J}}\mathbf{w}\|^2_{\mathbf{t}} + \mathbf{w}^{\mathbf{T}}\mathbf{B}_\xi\mathbf{P}_{\eta\zeta}(\widehat{\mathbf{A}}_{\mathbf{1w}}\mathbf{w} - \mathbf{2}\epsilon\widehat{\mathbf{F}}^{\mathbf{V}}_{\mathbf{w}}) + \mathbf{w}^{\mathbf{T}}\mathbf{B}_\eta\mathbf{P}_{\xi\zeta}(\widehat{\mathbf{A}}_{\mathbf{2w}}\mathbf{w} - \mathbf{2}\epsilon\widehat{\mathbf{G}}^{\mathbf{V}}_{\mathbf{w}}) + \mathbf{w}^{\mathbf{T}}\mathbf{B}_\zeta\mathbf{P}_{\xi\eta}(\widehat{\mathbf{A}}_{\mathbf{3w}}\mathbf{w} - \mathbf{2}\epsilon\widehat{\mathbf{H}}^{\mathbf{V}}_{\mathbf{w}}) + \mathbf{2}\epsilon\mathbf{DI} = 0. \tag{15}$$

(See [19] for more details.) **DI** denotes a positive quadratic term in the first-derivative difference approximations of the solution as in (11)

$$\mathbf{DI} = \left((\mathbf{D}_\xi\mathbf{w})^{\mathbf{T}}\mathbf{P}\widehat{\mathbf{F}}^{\mathbf{V}}_{\mathbf{w}} + (\mathbf{D}_\eta\mathbf{w})^{\mathbf{T}}\mathbf{P}\widehat{\mathbf{G}}^{\mathbf{V}}_{\mathbf{w}} + (\mathbf{D}_\zeta\mathbf{w})\mathbf{w}^{\mathbf{T}}\mathbf{P}\widehat{\mathbf{H}}^{\mathbf{V}}_{\mathbf{w}}\right) = \begin{pmatrix} \mathbf{D}_\xi\mathbf{w} \\ \mathbf{D}_\eta\mathbf{w} \\ \mathbf{D}_\zeta\mathbf{w} \end{pmatrix}^{\mathrm{T}} \widetilde{\mathbf{P}} \otimes \begin{pmatrix} \widehat{\mathbf{B}}_{\mathbf{11}} & \widehat{\mathbf{B}}_{\mathbf{12}} & \widehat{\mathbf{B}}_{\mathbf{13}} \\ \widehat{\mathbf{B}}_{\mathbf{21}} & \widehat{\mathbf{B}}_{\mathbf{22}} & \widehat{\mathbf{B}}_{\mathbf{23}} \\ \widehat{\mathbf{B}}_{\mathbf{31}} & \widehat{\mathbf{B}}_{\mathbf{32}} & \widehat{\mathbf{B}}_{\mathbf{33}} \end{pmatrix} \begin{pmatrix} \mathbf{D}_\xi\mathbf{w} \\ \mathbf{D}_\eta\mathbf{w} \\ \mathbf{D}_\zeta\mathbf{w} \end{pmatrix}, \tag{16}$$

where we have used the block-diagonal matrix $\widetilde{\mathbf{P}} = \mathrm{diag}(\mathbf{P}, \mathbf{P}, \mathbf{P})$ and

$$\widehat{\mathbf{B}}_{\mathbf{ij}} = I_\zeta \otimes I_\eta \otimes I_\xi \otimes \begin{pmatrix} \widehat{B}_{11} & \widehat{B}_{12} & \widehat{B}_{13} \\ \widehat{B}_{21} & \widehat{B}_{22} & \widehat{B}_{23} \\ \widehat{B}_{31} & \widehat{B}_{32} & \widehat{B}_{33} \end{pmatrix}. \tag{17}$$

Hence, positive semidefiniteness of DI follows directly from the positivity of $[\widehat{B}_{ij}]$.

Eq. (15) corresponds exactly to (11). $\mathbf{B}_{\xi,\eta,\zeta}$ picks the boundary terms in the respective directions. To keep the algebra to a minimum we focus on $\xi = 0$ and assume that all other boundary terms are 0 (i.e we assume that they are stable).

$$\|\sqrt{\mathbf{J}}\mathbf{w}\|_{\mathbf{t}}^{\mathbf{2}} - \mathbf{w}^{\mathbf{T}}\mathbf{E}_{0\xi}\mathbf{P}_{\eta\zeta}(\widehat{\mathbf{A}}_{\mathbf{1w}}\mathbf{w} - 2\epsilon\mathbf{F}_{\mathbf{w}}^{\mathbf{V}}) + 2\epsilon\mathbf{DI} = 0. \tag{18}$$

Since $\widehat{A}_{1w}$ is symmetric there is an orthonormal matrix X such that $\widehat{A}_{1w}X = X\widehat{\Lambda}_1$ where $\Lambda_1 = \mathrm{diag}(u_n, u_n, u_n, u_n + c, u_n - c)$ and u_n is the component of the velocity normal to the boundary. Moreover, we note that $X^{\mathrm{T}}X = I$.

2.5. Discrete wall boundary condition

Based on the one-dimensional analysis of the advection–diffusion equation, we construct two terms that are 0 to truncation error that we add to the right-hand side of (14).

$$\text{penalty} = \sigma^{\mathrm{I1}}(\mathbf{P}_{\xi}^{-\mathbf{1}}\mathbf{E}_{0\xi}\widehat{\mathbf{A}}'_{\mathbf{1w}}(\mathbf{w} - \mathbf{g}_{\mathbf{w}}^{\mathbf{I1}})) + \epsilon\sigma^{\mathrm{I2}}(\mathbf{P}_{\xi}^{-\mathbf{1}}\mathbf{E}_{0\xi}\widehat{\mathbf{I}}(\mathbf{w} - \mathbf{g}_{\mathbf{w}}^{\mathbf{I2}})). \tag{19}$$

Carrying the terms through the derivation they would appear on the right-hand side of (18) as

$$2\sigma^{\mathrm{I1}}(\mathbf{w}^{\mathbf{T}}\mathbf{E}_{0\xi}\mathbf{P}_{\eta\zeta}\widehat{\mathbf{A}}'_{\mathbf{1}}(\mathbf{w} - \mathbf{g}_{\mathbf{w}}^{\mathbf{I1}})) + 2\epsilon\sigma^{\mathrm{I2}}(\mathbf{w}^{\mathbf{T}}\mathbf{E}_{0\xi}\mathbf{P}_{\eta\zeta}\widehat{\mathbf{I}}(\mathbf{w} - \mathbf{g}_{\mathbf{w}}^{\mathbf{I2}})). \tag{20}$$

where $\widehat{\mathbf{I}} = (I_\zeta \otimes I_\eta \otimes I_\xi \otimes I_5)$. Note that, this particular splitting has a rationale from the equation point of view as well. The first term in (19) or (20) is the penalty term that would be used if $\epsilon = 0$ and the Euler equations were considered. The second term is the term that appears due to the viscosity in the equations. Based on this observation we will construct $\mathbf{g}_{\mathbf{w}}^{\mathbf{I1,2}}$ differently.

To construct the data vectors, we first note that for simple implementation $\mathbf{g}_{\mathbf{w}}^{\mathbf{I1,2}}$ need to have a value at every position. Hence, we copy $\mathbf{w}$ into $\mathbf{g}_{\mathbf{w}}^{\mathbf{I1,2}}$, which results in no boundary condition at all since the penalty terms vanish entirely. Then, we substitute into $\mathbf{g}_{\mathbf{w}}^{\mathbf{I1,2}}$ the correct boundary conditions. Hence, $\mathbf{w} - \mathbf{g}_{\mathbf{w}}^{\mathbf{I1,2}}$ will enforce the boundary conditions we wish. At the (k, l) boundary point at $\xi = 0$ we have that

$$w^{0kl:} = \left(\frac{a}{\sqrt{\bar{\gamma}}}\rho^{0kl}, u_1^{0kl}, u_2^{0kl}, u_3^{0kl}, \frac{1}{\sqrt{\gamma(\gamma-1)a}}T^{0kl}\right)^{\mathrm{T}} \tag{21}$$

and we construct g^{I2} substituting the boundary conditions into (21) to obtain

$$(g_w^{\mathrm{I2}})^{0kl:} = \left(\frac{a}{\sqrt{\bar{\gamma}}}\rho^{0kl}, 0, 0, 0, 0\right)^{\mathrm{T}}.$$

This means that there are four boundary conditions just as required at a wall. On the other hand, we construct g^{I1} by subtracting the normal component $(u_1, u_2, u_3)\cdot(n_1, n_2, n_3)$, from w. This condition is the wall boundary condition for the Euler equations. Setting the wall normal component to 0 is a subcondition of the no-slip condition and we have not overspecified the system. We could just as well have put g^{I1} to equal g^{I2} but we want to ensure that the solution converges to the Euler solution if the viscosity vanishes.

We add the penalty terms (20) to the right-hand side of (18),

$$\|\sqrt{\mathbf{J}}\mathbf{w}\|_{\mathbf{t}}^{\mathbf{2}} - \mathbf{w}^{\mathbf{T}}\mathbf{E}_{0\xi}\mathbf{P}_{\eta\zeta}(\widehat{\mathbf{A}}_{\mathbf{1w}}\mathbf{w} - \mathbf{2}\epsilon\mathbf{F}_{\mathbf{w}}^{\mathbf{V}}) + \mathbf{2}\epsilon\mathbf{DI} = 2\sigma^{\mathrm{I1}}(\mathbf{w}^{\mathbf{T}}\mathbf{E}_{0\xi}\mathbf{P}_{\eta\zeta}\widehat{\mathbf{A}}'_{\mathbf{1}}(\mathbf{w} - \mathbf{g}^{\mathbf{I1}})) + 2\epsilon\sigma^{\mathrm{I2}}(\mathbf{w}^{\mathbf{T}}\mathbf{E}_{0\xi}\mathbf{P}_{\eta\zeta}\widehat{\mathbf{I}}(\mathbf{w} - \mathbf{g}^{\mathbf{I2}})).$$

Or, by introducing, $(w^1)^{ijk:} = (\tilde{w})^{ijk:} - (g_w^{\mathrm{I1}})^{ijk:}$ and $(w^2)^{ijk:} = (\tilde{w})^{ijk:} - (g_w^{\mathrm{I2}})^{ijk:}$, and noting that the first component of $(w^{1,2})^{ijk:}$ is zero,

$$\|\sqrt{\mathbf{J}}\mathbf{w}\|_{\mathbf{t}}^{\mathbf{2}} - \mathbf{w}^{\mathbf{T}}\mathbf{E}_{0\xi}\mathbf{P}_{\eta\zeta}(\widehat{\mathbf{A}}_{\mathbf{1w}}\mathbf{w} + 2\sigma^{\mathrm{I1}}\widehat{\mathbf{A}}'_{\mathbf{1w}}\mathbf{w}^{\mathbf{1}}) + 2\epsilon\mathbf{w}^{\mathbf{T}}\mathbf{E}_{0\xi}\mathbf{P}_{\eta\zeta}\mathbf{F}_{\mathbf{w}}^{\mathbf{V}} - 2\epsilon\sigma^{\mathrm{I2}}(\mathbf{w}^{\mathbf{T}}\mathbf{E}_{0\xi}\widehat{\mathbf{I}}\mathbf{w}^{\mathbf{2}}) + 2\epsilon\mathbf{DI} = 0.$$

The following lemma holds.

Lemma 2.2. *Let* $\widehat{A}_{1w} = X^{\mathrm{T}}\Lambda_1 X$ *where* $\Lambda_1 = \mathrm{diag}(u_n, u_n, u_n, u_n + a, u_n - a)$ *and* $u_n = (\xi_x u_1, \xi_y u_2, \xi_z u_3)/(\sqrt{\xi_x^2 + \xi_y^2 + \xi_z^2})$ *is the velocity component normal to the boundary and assume that* $u_n = 0$. *Then,* $\mathbf{w}^{\mathbf{T}}\mathbf{E}_{0\xi}\mathbf{P}_{\eta\zeta}(\widehat{\mathbf{A}}_{\mathbf{1w}}\mathbf{w} + 2\sigma^{\mathrm{I1}}\widehat{\mathbf{A}}'_{\mathbf{1w}}\mathbf{w}^{\mathbf{1}}) > 0$ *if*

1. $\sigma^{\mathrm{I1}} = -2$
2. $\widehat{\mathbf{A}}'_{\mathbf{1w}} = (I_\zeta \otimes I_\eta \otimes I_\xi \otimes X^{\mathrm{T}} \Lambda'_1 X)$
3. $\Lambda'_1 = \Lambda^+ = \mathrm{diag}(0,0,0,a,0)$.

Remark. Note that the Lemma 2.2 alone describes a stable penalty treatment of the no-penetration wall boundary condition for the Euler equations.

Proof. We require that

$$-\mathbf{w}^{\mathbf{T}}\mathbf{E}_{0\xi}\mathbf{P}_{\eta\zeta}(\widehat{\mathbf{A}}_{\mathbf{1w}}\mathbf{w} + 2\sigma^{\mathrm{I1}}\widehat{\mathbf{A}}'_{\mathbf{1w}}\mathbf{w}^{\mathbf{1}}) \tag{22}$$

is non-negative for stability. We make the transformation to characteristic variables using $\mathbf{X}^{\mathbf{T}} = (I_\zeta \otimes I_\eta \otimes I_\xi \otimes X^{\mathrm{T}})$ where $X^{\mathrm{T}}\widehat{A}_{1w}X = \Lambda_1 = \mathrm{diag}(u_n, u_n, u_n, u_n + a, u_n - a)$ and u_n is the normal component of the velocity. That is

$$-\mathbf{w}^{\mathbf{T}}\mathbf{X}\mathbf{X}^{\mathbf{T}}\mathbf{E}_{0\xi}\mathbf{P}_{\eta\zeta}(\widehat{\mathbf{A}}_{\mathbf{1w}}\mathbf{w} + 2\sigma^{\mathrm{I1}}\widehat{\mathbf{A}}'_{\mathbf{1w}}\mathbf{X}\mathbf{X}^{\mathbf{T}}\mathbf{w}^{\mathbf{1}}) = -\mathbf{c}^{\mathbf{T}}\mathbf{E}_{0\xi}\mathbf{P}_{\eta\zeta}(\widehat{\mathbf{\Lambda}}_{\mathbf{1}}\mathbf{c} + 2\sigma^{\mathrm{I1}}\widehat{\mathbf{\Lambda}}'_{\mathbf{1}}\mathbf{c}^{\mathbf{1}}), \tag{23}$$

where $\mathbf{c}^{\mathbf{1}} = (\mathbf{X}^{\mathbf{T}}\mathbf{w} - \mathbf{X}^{\mathbf{T}}\mathbf{g}^{\mathbf{I1}}_{\mathbf{w}}) = \mathbf{c} - \mathbf{g}^{\mathbf{C1}}$. Since $\widehat{A}_{1w}$ is a linear combination of A_1, A_2 and A_3 it suffices to consider the Cartesian case where $\widehat{A}_{1w} = A_1$, which simplifies the notation. In that case

$$X = \begin{pmatrix} 0 & 0 & -\sqrt{\frac{\gamma-1}{\gamma}} & \frac{1}{\sqrt{2\gamma}} & \frac{1}{\sqrt{2\gamma}} \\ 0 & 0 & 0 & \frac{1}{\sqrt{2\gamma}} & -\frac{1}{\sqrt{2\gamma}} \\ 1 & 0 & 0 & 0 & 0 \\ 0 & 1 & 0 & 0 & 0 \\ 0 & 0 & \frac{1}{\sqrt{\gamma}} & \sqrt{\frac{\gamma-1}{2\gamma}} & \sqrt{\frac{\gamma-1}{2\gamma}} \end{pmatrix}. \tag{24}$$

Let $c^{kl} = (c^{0kl1}, \ldots, c^{0kl5})^{\mathrm{T}}$, i.e., the vector of the variables at the (k,l)th boundary point at $x = 0$. Also, let $(w^1)^{kl}$ be defined in a same way. We rewrite (23) on component form

$$\sum_{kl} -c^{kl}P^j_\eta P^k_\zeta(\Lambda_1 c^{kl}) + 2\sigma^{\mathrm{I1}}\Lambda'_1(c^{kl} - (g^{C1})^{kl}). \tag{25}$$

Now (25) must be non-negative. That can only be satisfied if each term in the sum is non-negative and we continue to study the point k, l and drop the indices to simplify the notation. The variables are

$$c = \begin{pmatrix} \tilde{u}_3 \\ \tilde{u}_4 \\ -\sqrt{\frac{\gamma-1}{\gamma}}\frac{a}{\sqrt{\gamma}\rho}\tilde{\rho} + \frac{1}{\gamma\sqrt{\gamma-1}a}\widetilde{T} \\ \frac{a}{\rho\gamma\sqrt{2(\gamma-1)}}\tilde{\rho} + \frac{1}{\sqrt{2}}\tilde{u}_1 + \frac{1}{\sqrt{2\gamma}a}\widetilde{T} \\ \frac{a}{\rho\gamma\sqrt{2(\gamma-1)}}\tilde{\rho} - \frac{1}{\sqrt{2}}\tilde{u}_1 + \frac{1}{\sqrt{2\gamma}a}\widetilde{T} \end{pmatrix}. \tag{26}$$

We want to ensure that the solution converges to the Euler equations when $Re \to \infty$ and therefore we will only use the subcondition $u \cdot n = 0$. At $x = 0$ the boundary condition is $\tilde{u}_1 = u_1 = 0$. Hence, $\Lambda_1 = \mathrm{diag}(0,0,0,a,-a)$.

Next, we turn to the construction of g^{C1}. Inserting the condition $\tilde{u}_1 = 0$ in (26) gives us

$$g^{C1} = \begin{pmatrix} \tilde{u}_3 \\ \tilde{u}_4 \\ -\sqrt{\frac{\gamma-1}{\gamma}}\frac{a}{\sqrt{\gamma}\rho}\tilde{\rho} + \frac{1}{\gamma\sqrt{\gamma-1}a}\widetilde{T} \\ \frac{a}{\rho\gamma\sqrt{2(\gamma-1)}}\tilde{\rho} + \frac{1}{\sqrt{2\gamma}a}\widetilde{T} \\ \frac{a}{\rho\gamma\sqrt{2(\gamma-1)}}\tilde{\rho} + \frac{1}{\sqrt{2\gamma}a}\widetilde{T} \end{pmatrix}. \tag{27}$$

(This choice of g^{C1} implies that $(c - g^{C1}) = (0, 0, 0, \tilde{u}_1, -\tilde{u}_1)/\sqrt{2}$ ensuring that the correct boundary condition is enforced irrespective of the choice of Λ'.) To prove boundedness we will make use of the observation that

$$g^{C1} = (\tilde{c}_1, \tilde{c}_2, \tilde{c}_3, (c_4 + c_5)/2, (c_4 + c_5)/2)^{\mathrm{T}}. \tag{28}$$

Up until now, we have made sure that only the Euler subset of the no-slip boundary condition is used to bound the inviscid boundary terms.

Next, we will turn to the choice of Λ' and we will restrict ourselves to a specific form. The purpose is to make the wall boundary procedure similar to the far-field boundary procedure. For the far-field boundary conditions we penalize the ingoing characteristics and the viscous flux (see [19]). From a programming point of view it would be very convenient if it was possible to have the same treatment of the inviscid portion of the wall boundary conditions (i.e., we would be able to use the same routine and minimize the complexity in the program as well as runtime). Hence, we will try the following ansatz, $\Lambda' = \Lambda^+ = \mathrm{diag}(0, 0, 0, a, 0)$, which gives us a penalty term for the ingoing characteristic variable only. We rewrite (25) as

$$-\tilde{c}^{\mathrm{T}}\Lambda_1\tilde{c} + 2\sigma^{\mathrm{I1}}\tilde{c}^{\mathrm{T}}\Lambda(\tilde{c} - g^{C1}) = -c_4^2 a + c_5^2 a - 2\sigma_1 c_4 a(c_4 - g_4^{\mathrm{I1}}) = a(-c_4^2 + c_5^2) - \sigma_1 c_4(c_4 - c_5) > 0,$$

where $(g^{C1})_4 = (c_4 + c_5)/2$ was used in the last step. Choosing $\sigma_1 = -2$ leads to

$$a(c_4 - c_5)^2 > 0. \qquad \square$$

Using Lemma 2.2 we are left with,

$$\|\sqrt{\mathbf{J}}\mathbf{w}\|_{\mathbf{t}}^{\mathbf{2}} + 2\epsilon\mathbf{w}^{\mathbf{T}}\mathbf{E}_{0\xi}\mathbf{P}_{\eta\zeta}\mathbf{F}_{\mathbf{w}}^{\mathbf{V}} - 2\epsilon\sigma^{\mathrm{I2}}(\mathbf{w}^{\mathbf{T}}\mathbf{E}_{0\xi}\widehat{\mathbf{I}}(\mathbf{w} - \mathbf{g}^{\mathbf{I2}})) + 2\epsilon\mathbf{DI} \leqslant 0. \tag{29}$$

Just as for the advection–diffusion equation, we need to borrow from **DI** to obtain a quadratic form in boundary terms. In complete analogy with (4) we write,

$$\mathbf{DI} = \widetilde{\mathbf{P}} \otimes [\widehat{\mathbf{B}}_{\mathbf{ij}}] = \sum_{i=0}^{N} p_{\xi i}\widetilde{\mathbf{P}}'_{\eta\zeta} \otimes [\widehat{\mathbf{B}}_{\mathbf{ij}}] = p_{\xi 0}\widetilde{\mathbf{P}}'_{\eta\zeta} \otimes [\widehat{\mathbf{B}}_{\mathbf{ij}}] + \widetilde{\mathbf{DI}}, \tag{30}$$

where $p_{\xi i}$ are the non-zero elements of the diagonal matrix P_ξ and $\widetilde{\mathbf{P}}'_{\eta\zeta} = \mathrm{diag}(\mathbf{P}_{\eta\zeta}, \mathbf{P}_{\eta\zeta}, \mathbf{P}_{\eta\zeta})$. Next, we estimate (29) as

$$\|\sqrt{\mathbf{J}}\mathbf{w}\|_{\mathbf{t}}^{\mathbf{2}} + \epsilon\mathbf{q}^{\mathbf{T}}\widetilde{\mathbf{P}}_{\eta\zeta} \otimes \begin{pmatrix} -2\sigma^{\mathrm{I2}}\widehat{\mathbf{I}} & \widehat{\mathbf{B}}_{\mathbf{11}} & \widehat{\mathbf{B}}_{\mathbf{12}} & \widehat{\mathbf{B}}_{\mathbf{13}} \\ \widehat{\mathbf{B}}_{\mathbf{11}} & 2p_{\xi 0}\widehat{\mathbf{B}}_{\mathbf{11}} & 2p_{\xi 0}\widehat{\mathbf{B}}_{\mathbf{12}} & 2p_{\xi 0}\widehat{\mathbf{B}}_{\mathbf{13}} \\ \widehat{\mathbf{B}}_{\mathbf{12}} & 2p_{\xi 0}\widehat{\mathbf{B}}_{\mathbf{12}} & 2p_{\xi 0}\widehat{\mathbf{B}}_{\mathbf{22}} & 2p_{\xi 0}\widehat{\mathbf{B}}_{\mathbf{23}} \\ \widehat{\mathbf{B}}_{\mathbf{13}} & 2p_{\xi 0}\widehat{\mathbf{B}}_{\mathbf{13}} & 2p_{\xi 0}\widehat{\mathbf{B}}_{\mathbf{32}} & 2p_{\xi 0}\widehat{\mathbf{B}}_{\mathbf{33}} \end{pmatrix}\mathbf{q}' \leqslant 0 \tag{31}$$

by throwing away $2\epsilon\tilde{D}I$. In (31) we have introduced $\widetilde{\mathbf{P}}_{\eta\zeta} = \mathrm{diag}(\mathbf{P}_{\eta\zeta}, \mathbf{P}_{\eta\zeta}, \mathbf{P}_{\eta\zeta}, \mathbf{P}_{\eta\zeta})$ and

$$\mathbf{q}^{\mathbf{T}} = ((\mathbf{w}_{0\xi})^{\mathbf{T}}, (\mathbf{D}_\xi\mathbf{w})_{0\xi}^{\mathbf{T}}, (\mathbf{D}_\eta\mathbf{w})_{0\xi}^{\mathbf{T}}, (\mathbf{D}_\zeta\mathbf{w})_{0\xi}^{\mathbf{T}}),$$
$$(\mathbf{q}')^{\mathbf{T}} = ((\mathbf{w}^{\mathbf{2}})_{0\xi}^{\mathbf{T}}, (\mathbf{D}_\xi\mathbf{w})_{0\xi}^{\mathbf{T}}, (\mathbf{D}_\eta\mathbf{w})_{0\xi}^{\mathbf{T}}, (\mathbf{D}_\zeta\mathbf{w})_{0\xi}^{\mathbf{T}}).$$

Note that, $p_{\xi 0}$ is of order $\mathcal{O}(\Delta\xi)$. Stability is achieved if the matrix in (31) is positive definite. The following theorem is the main theoretical result of this article.

Theorem 2.3. *The scheme is stable if* Lemma 2.2 *holds and*

$$\sigma^{\mathrm{I2}} \leqslant -\frac{1}{4p_{\xi 0}}\max\left(\frac{\gamma\mu}{Pr\rho}, \frac{5\mu}{3\rho}\right).$$

Proof. In Eq. (31) the following expression needs to be positive

$$\mathbf{q}^{\mathbf{T}}\widetilde{\mathbf{P}}_{\eta\zeta} \otimes \mathbf{M}\mathbf{q}'. \tag{32}$$

Note that, $\mathbf{M} = I_\zeta \otimes I_\eta \otimes I_\xi \otimes M$, where

$$M = \begin{pmatrix} -2\sigma^{\mathrm{I2}}\widehat{I}_5 & \widehat{B}_{11} & \widehat{B}_{12} & \widehat{B}_{13} \\ \widehat{B}_{11} & 2p_{\xi 0}\widehat{B}_{11} & 2p_{\xi 0}\widehat{B}_{12} & 2p_{\xi 0}\widehat{B}_{13} \\ \widehat{B}_{12} & 2p_{\xi 0}\widehat{B}_{12} & 2p_{\xi 0}\widehat{B}_{22} & 2p_{\xi 0}\widehat{B}_{23} \\ \widehat{B}_{13} & 2p_{\xi 0}\widehat{B}_{13} & 2p_{\xi 0}\widehat{B}_{32} & 2p_{\xi 0}\widehat{B}_{33} \end{pmatrix} \tag{33}$$

is a 20×20 matrix. It is only the ρ-components $(\mathbf{q}')^{0::1}$ that differs from $\mathbf{q}$. All other components are equal in $\mathbf{q}$ and $\mathbf{q}'$. Moreover, the rows/columns of $\mathbf{M}$ corresponding to the ρ-components are all 0 (since the first component of the viscous flux is 0) and does not affect the positivity of (32). Hence, we may instead of (32) consider

$$\mathbf{q}^{\mathrm{T}}\widetilde{\mathbf{P}}_{\eta\zeta} \otimes \mathbf{M}\mathbf{q}. \tag{34}$$

For stability we have to determine σ^{I2} (below denoted σ) such that M is positive semidefinite. Again, we will restrict ourselves to the Cartesian case and the boundary at $x = 0$ to simplify the notation. (We denote $p_{\xi 0} = p_0$.) It turns out that it is difficult to derive sharp estimates on σ using the form (34). Instead, we expand the problem to

$$\widetilde{M} = \begin{pmatrix} -2\sigma I_{15} & \widehat{B} \\ \widehat{B} & 2p_0\widehat{B} \end{pmatrix}, \tag{35}$$

where $\widehat{B} = [\widehat{B}_{ij}]$ and I_{15} is the 15×15 identity matrix. If $\widetilde{M}$ is positive semidefinite then all its principal submatrices are (see [5]). One of the submatrices is M. Letting v be an arbitrary vector we may rotate $\widetilde{M}$ with a non-singular matrix R.

$$v^{\mathrm{T}}R^{T,-1}R^{\mathrm{T}}\widetilde{M}RR^{-1}v. \tag{36}$$

Denote $w = R^{-1}v$ and $\widehat{M} = R^{\mathrm{T}}\widetilde{M}R$. The task is now to choose σ such that $\widehat{M}$ is positive semi-definite. We make the particular choice

$$R = \begin{pmatrix} I_{15} & \alpha \\ 0 & I_{15} \end{pmatrix}, \quad \alpha = \frac{1}{2\sigma}\widehat{B}$$

and require that $\sigma \neq 0$. Then

$$\widehat{M} = \begin{pmatrix} -2\sigma I_{15} & 0 \\ 0 & \frac{1}{2\sigma}\widehat{B}^2 + 2p_0\widehat{B} \end{pmatrix}.$$

Obviously, σ must be negative and since B is symmetric and positive semidefinite the condition is now

$$\frac{1}{2\sigma}\widehat{B} + 2p_0 I_{15} \geqslant 0.$$

Again, using the symmetry of $\widehat{B}$ we have $\widehat{B} = X^{\mathrm{T}}\widehat{\Lambda^B}X$ where $X^{\mathrm{T}}X = I_{15}$. Hence, by noting that

$$\frac{1}{2\sigma}\widehat{B} + 2p_0 I_{15} = X^{\mathrm{T}}\left(-\frac{1}{2\sigma}\widehat{\Lambda^B} + 2p_0 I_{15}\right)X,$$

we require that $\frac{1}{2\sigma}\widehat{\lambda_i^B} + 2p_0 \geqslant 0$, which implies that

$$\sigma \leqslant -\frac{1}{4p_0}\widehat{\lambda_i^B}, \quad i = 1, \ldots, 15. \tag{37}$$

The remaining task is to determine the eigenvalues of $\widehat{B}$. We begin with a few observations. Row/column 1, 6, 11 of the matrix $\widehat{B}$ have no non-zero entries (since the first components of the viscous fluxes are 0) and correspond to three eigenvalues equal to 0. Row/column 5, 10, 15 have only the diagonal entry non-zero and equal to $(Pr\rho)/(\gamma\mu)$, which is the value of three more eigenvalues. The remaining 9×9 matrix (using $\lambda = -2\mu/3$) is

$$\frac{\mu}{\rho}\begin{pmatrix}
\frac{4}{3} & 0 & 0 & 0 & \frac{1}{6} & 0 & 0 & 0 & \frac{1}{6} \\
0 & 1 & 0 & \frac{1}{6} & 0 & 0 & 0 & 0 & 0 \\
0 & 0 & 1 & 0 & 0 & 0 & \frac{1}{6} & 0 & 0 \\
0 & \frac{1}{6} & 0 & 1 & 0 & 0 & 0 & 0 & 0 \\
\frac{1}{6} & 0 & 0 & 0 & \frac{4}{3} & 0 & 0 & 0 & \frac{1}{6} \\
0 & 0 & 0 & 0 & 0 & 1 & 0 & \frac{1}{6} & 0 \\
0 & 0 & \frac{1}{6} & 0 & 0 & 0 & 1 & 0 & 0 \\
0 & 0 & 0 & 0 & 0 & \frac{1}{6} & 0 & 1 & 0 \\
\frac{1}{6} & 0 & 0 & 0 & \frac{1}{6} & 0 & 0 & 0 & \frac{4}{3}
\end{pmatrix}.$$

The eigenvalues of $\widehat{B}$ are: $\frac{\mu}{\rho}\{\frac{5}{3},\frac{5}{6},\frac{5}{6},\frac{7}{6},\frac{7}{6},\frac{7}{6},\frac{7}{6},\frac{7}{6},0,0,0,\frac{\gamma}{Pr},\frac{\gamma}{Pr},\frac{\gamma}{Pr}\}$. Taking the maximum of the eigenvalues in the condition (37) proves the theorem. □

Remark. Note that the extension of M to $\widetilde{M}$ makes the proof valid for a y or z boundary as well, since their stability would be determined by two other submatrices of $\widetilde{M}$.

We close this section with a few comments on the implementation and interpretation of the present scheme. The symmetric form of the linearized equations serves as an analytical tool to derive well-posed boundary conditions. In a program it is more convenient to transform the boundary terms to the characteristic form directly from the conservative formulation and compute all the penalty terms that act on the variables (and not the viscous fluxes). The form of the first penalty term bounding the inviscid flux was derived in characteristic space and that can be directly applied. (The same is true for a far-field boundary and the same routine can be used as mentioned earlier. See for example [17] for transformation matrices.) In the case of a wall the extra penalty term can also be computed in characteristic space by observing that there is an orthonormal transformation from symmetric variables to characteristic variables. The penalty term in (29) stated in symmetric variables can be rewritten as $-2\epsilon\sigma^{I2}(\mathbf{w}^{\mathbf{T}}\mathbf{E}_{0\xi}\widehat{\mathbf{I}}(\mathbf{w}-\mathbf{g}^{\mathbf{I2}})) = 2\epsilon\sigma^{I2}(\mathbf{c}^{\mathbf{T}}\mathbf{E}_{0\xi}\widehat{\mathbf{I}}(\mathbf{c}-\mathbf{g}^{\mathbf{C2}}))$ where $\mathbf{g}^{\mathbf{C2}}$ is the transformed data vector. Hence, the penalty matrix will appear as an identity matrix in characteristic space as well. This makes it easy to treat the entire wall boundary condition and the inviscid part of the far-field boundary condition in characteristic space and use the same routine.

Finally, there are many different choices when constructing $\widehat{A}_1'$ all valid from the linear analysis. We may construct the matrix using u_{boundary} or g^{I1} or any average of the two. We choose $\widehat{A}_1'$ to be the ingoing portion of the Roe-averaged $\widehat{A}_1$, i.e. $\widehat{F}^1(u_{\text{boundary}}) - \widehat{F}^I(g^i) = \widehat{A}_1(u_{\text{boundary}}, g^{\text{I}})(u_{\text{boundary}} - g^{\text{I}})$ (see [18]), which may be advantageous in an extension to allow non-smooth solutions. In Appendix A there is a flow chart explaining step-by-step how to proceed when implementing this scheme.

3. Computation of cylinder in free stream

In [21] an analytical viscous shock solution was computed on a two-block grid using this technique. It was shown that the theoretical convergence rates were obtained for the different orders of accuracy available. We conclude without restating those results that the numerical procedure, as well as the current implementation, has a verifiable order of accuracy.

3.1. Effect of wall penalty

The weak enforcement of the boundary conditions using penalty terms does not force the numerical solution to exactly fulfill the boundary conditions. Instead the effect can be described as a rubber-band pulling the solution towards the boundary condition.

To demonstrate the rubber-band effect of the wall penalty terms, we show a sequence of vector plots of the velocities near the wall at the upper-left part of the cylinder, see Figs. 1 and 2. The governing flow parameters

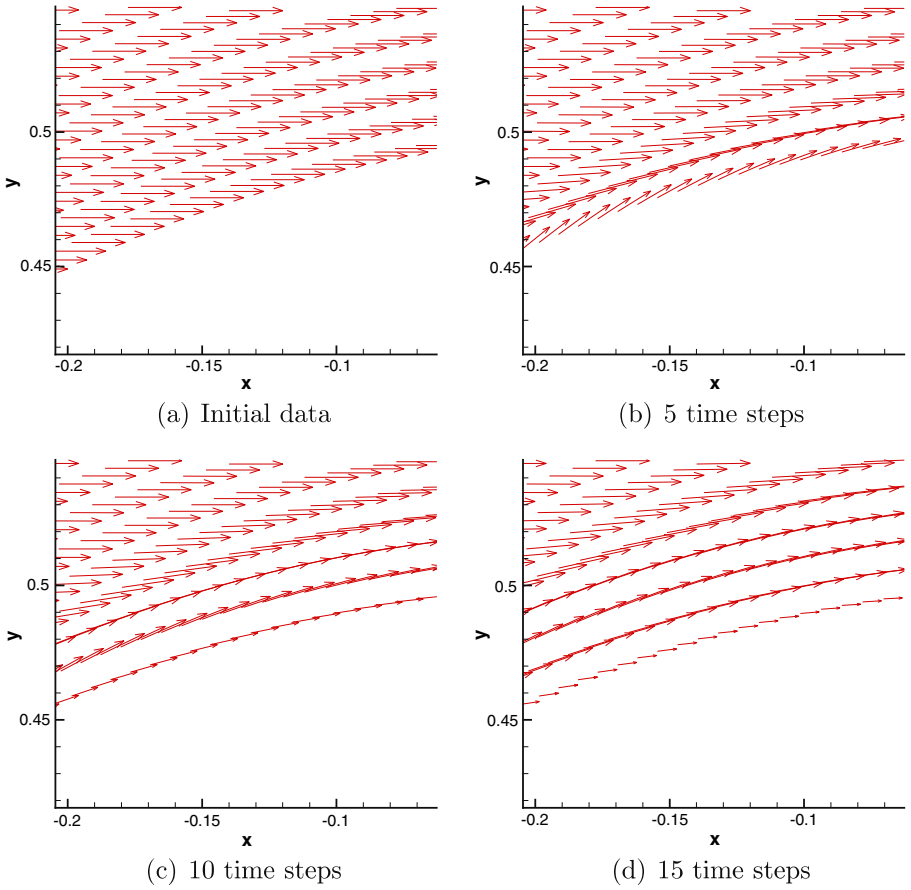

Fig. 1. Vector plots of the u and v velocities computed with a 3rd-order scheme.

are $Ma = 0.1$ and $Re = 100$. (This is the flow case used in all the computations below.) The initial condition is a constant free stream in the entire domain, which does not satisfy the no-slip boundary condition. The velocity vectors are oscillating with decreasing amplitude around the slip condition and at the same time decreasing their lengths to satisfy the no-slip condition. The effect clearly relates to the two penalty terms used to enforce the full wall boundary condition. Already at 30 time steps the arrows are so short that they are hardly visible.

The penalty procedure is the main reason for the robustness. The numerical solution remains smooth and no high-frequency oscillations are triggered despite incompatible data.

In contrast to the penalty technique, we also enforced the boundary conditions at the wall in a more standard way. We updated the solution in the entire domain omitting the penalty terms at the wall and after each stage in the Runge–Kutta scheme we overwrote the solution at the wall using the exact boundary values. We initiated the cylinder computation with a homogeneous free-stream (as above) and kept everything else the same. With that setup, all schemes became unstable. However, the commonly used second-order scheme could be stabilized with an order of magnitude increase of the artificial diffusion. Obviously, that approach also decreases the accuracy of the solution. The high-order schemes were impossible to stabilize with extra diffusion.

3.2. Accuracy

It may be argued that one should exactly enforce the wall boundary conditions since we have known data at hand. But by doing so (and for the moment disregarding the crucial stability issue), errors may increase elsewhere. Typically at locations where the exact solution is not known and hence the error is impossible

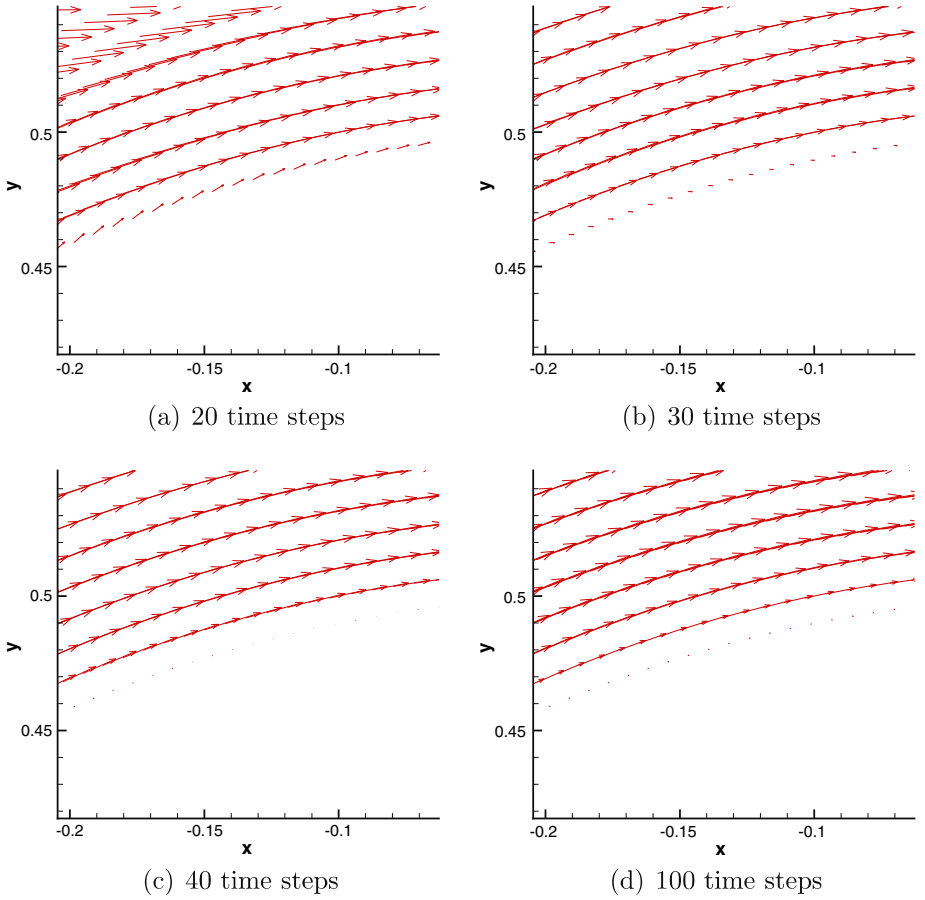

Fig. 2. Vector plots of the u and v velocities computed with a 3rd-order scheme. The last plot corresponds to $T \approx 0.31$.

to measure. The weak imposition clearly shows the errors at the boundary and serves as a rough measure of the error of the entire solution.

We compute on the full grid (fine) and on every other grid point in both directions (medium) and on every fourth (coarse). We measure the maximum error in u and v on the upper wall of the cylinder at $T = 1.0$. The convergence rates of u and v, denoted q_u and q_v, are computed for four different orders of accuracy (2, 3, 4, 5). The results are seen in Tables 1 and 2. We emphasize a few observations. Firstly, in all cases but one (the v velocity for 4th- and 5th-order schemes on the medium grid) an increase in formal order results in increased accuracy on all grids. Even on the coarse grid. Secondly, the general trend is that higher theoretical order of accuracy yields a higher convergence rate in the computations. There are exceptions here too, but we point out that convergence rates on model problems are usually shown on much finer grids than the fine grid in this test case and one should not expect these results to be on the asymptotic slope yet. Nevertheless, even on these more realistic CFD grids, the convergence rates are not too far off from their theoretical values between the medium and fine grid.

It is sometimes argued that a low-order method should perform better on coarse grids. The idea is that h^4 quickly becomes larger than h^2 if h increases. This is clearly not the case in our experiments.

Table 1
Maximum errors on the wall and convergence rates in u at $T = 1$, for $Re = 100$ and $Ma = 0.1$ and different orders of accuracy

e_u order	2	q_u	3	q_u	4	q_u	5	q_u
Coarse	0.145	–	9.93e−2	–	6.70e−2	–	3.88e−2	–
Medium	4.61e−2	1.7	1.04e−2	3.2	9.54e−3	2.8	8.66e−3	2.2
Fine	6.41e−3	2.8	1.33e−3	3.0	4.41e−4	4.4	1.72e−4	5.7

Table 2
Maximum errors on the wall and convergence rates in v at $T = 1$, for $Re = 50$ and $Ma = 0.5$ and different orders of accuracy

e_v order	2	q_v	3	q_v	4	q_v	5	q_v
Coarse	0.114	–	7.50e−2	–	4.24e−2	–	2.49e−2	–
Medium	3.31e−2	1.8	1.42e−2	2.4	5.74e−3	2.9	8.12e−3	1.6
Fine	5.31e−3	2.6	1.13e−3	3.7	4.08e−4	3.8	1.96e−4	5.4

A heuristic explanation why the high-order methods are more accurate on coarse grids would be that a high-order method will resolve high-frequency oscillations better than a low-order scheme. In this case the high-frequency contents of the solution describes a sharp gradient (the boundary layer). The pull towards 0 subject to the penalty is the same for all orders, but the pull away from 0 is less for a high-order method because it captures the gradient more accurately on any grid. Hence, a better accuracy at the boundary points for higher-order. This argument also explains our claim that the errors at the boundary points reflect the overall error of the solution.

The reverse order argument discussed above fails since the order of accuracy is the limiting slope as $h \to 0$. When following the error backwards to coarser grids one will at some point pass a kink and start following a slope of lower order. This implies that the high-order scheme is in general more accurate even on underresolved grids.

3.3. Vortex shedding in free stream

As a next test case, we will calculate the flow around a circular cylinder. Again, with the free-stream Mach number 0.1 and the Reynolds number based on the diameter of the cylinder set to 100. This case has been thoroughly studied and both experimental data and computational results are available in the literature. We excite the shedding by inserting a vortex in front of the cylinder. We run until $T = 1000$ where we have a steady shedding going and measure flow characteristics between $T = 1000 - 1500$.

We measure the following quantities: The Strouhal number, $St = \frac{fL}{V}$ where f is the frequency of the vortex shedding. L is the characteristic length (in this case the diameter of the cylinder, which is 1) V is the free-stream velocity of the fluid and is 0.1 in this case. Further, we will compute the pressure lift, pressure drag, viscous lift and viscous drag coefficients. (We compute the forces as approximate line integrals and non-dimensionalize by the dynamic pressure times the diameter, D, of the cylinder: $\frac{1}{2}\rho_\infty V^2 D$.) The sum of the viscous and pressure lift/drag becomes the lift/drag coefficients. All coefficients will be presented with its maximal, minimal value as well as its average value taken over all measure points (except St which is a frequency).

Two different base grids will be used. Grid 1 in Fig. 3 is a five-block grid with 101×201 grid points in each block. It has 4×101 grid points on the cylinder circumference and 201 points in the radial direction. Grid 1 is smaller and will only be used in Case 1 below. It is included to quantify the effect from the far-field boundaries.

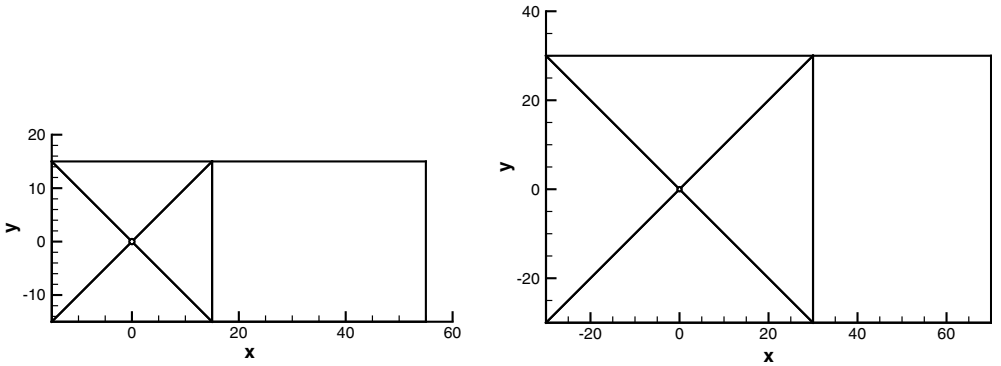

(a) Grid 1 (b) Grid 2

Fig. 3. Block structure and sizes of computational grids.

Grid 2 is the five-block grid in Fig. 3. It has a larger domain but the same number of points in each block and in the circumferential and radial direction. The smallest cell size close to the cylinder is the same meaning that the stretching in the radial direction is slightly larger to account for the increased domain size. (Grid 2, or subsets of it, is used in Cases 2–7 where we use the notation *circumferential* × *radial* to indicate the number of points in each direction around the cylinder.) We compute seven different cases.

1. Grid 1 and a 3rd-order schemes. Results are shown in Table 3.
2. Every 4th point of Grid 2 (101 × 51) and the 3rd-order scheme. The results are shown in Table 4. In Fig. 4 a vector plot of the velocity near a small portion of the cylinder surface is shown.
3. Every 2nd point of Grid 2 (201 × 101) and the 3rd-order scheme. The results are shown in Table 5.
4. Every point of Grid 2 (401 × 201) and the 3rd-order scheme. The results are shown in Table 6.
5. Every 4th point of Grid 2 (101 × 51) and the 5th-order scheme. The results are shown in Table 7. In Fig. 4, a vector plot of the velocity near a small part of the cylinder surface.
6. Every 2nd point of Grid 2 (201 × 101) and the 5th-order scheme. The results are shown in Table 8.
7. Every point of Grid 2 (401 × 201) and the 5th-order scheme. The results are shown in Table 9 and in Fig. 5, the ρu variable of the solution at $T = 1500$ is shown.

In Table 10 we show reference data from [24,8,6]. It is only Case 2 that deviates a bit from the reference data and all other agrees well. Case 2 is the least resolved case with the lowest order and naturally the least accurate of all computations. But note that the 5th-order scheme with the same resolution (Case 5) compares

Table 3
Data for Case 1

	Lift	Drag	pfx	pfy	visx	visy	Strouhal
Max	0.3316	1.3701	1.0242	0.2924	0.3460	0.0442	–
Min	−0.3317	1.3508	1.0067	−0.2925	0.3440	−0.0442	–
Mean	0.0067	1.3603	1.0153	0.0054	0.3450	0.0013	0.167

pfx, pfy, visx, visy are pressure and shear stress forces in the x- and y-direction acting on the cylinder.

Table 4
Data for Case 2

	Lift	Drag	pfx	pfy	visx	visy	Strouhal
Max	0.3433	1.3016	1.0492	0.3225	0.2527	0.0304	–
Min	−0.3435	1.2807	1.0289	−0.3226	0.2515	−0.0304	–
Mean	0.0077	1.2911	1.0390	0.0066	0.2521	0.0010	0.0154

pfx, pfy, visx, visy are pressure and shear stress forces in the x- and y-direction acting on the cylinder.

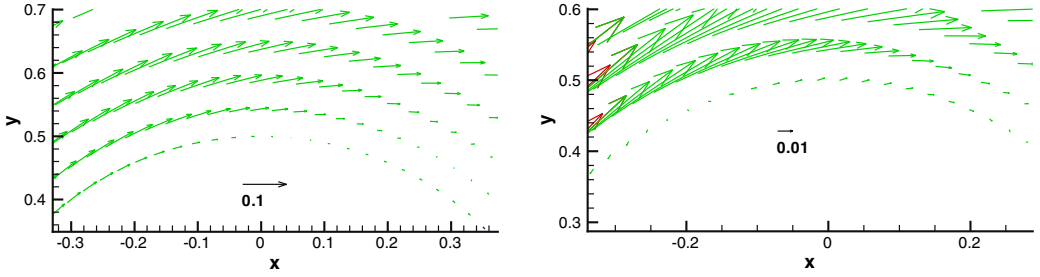

(a) Case 2, 3rd-order (b) Case 5, 5th-order

Fig. 4. Plots of solutions of Case 2 and Case 5 at $T = 1500$. Velocity vectors close to the upper wall of the cylinder including reference vectors of length 0.01.

Table 5
Data for Case 3

	Lift	Drag	pfx	pfy	visx	visy	Strouhal
Max	0.3294	1.3404	1.0172	0.2946	0.3235	0.0407	–
Min	−0.3296	1.3214	0.9996	−0.2947	0.3217	−0.0407	–
Mean	0.0046	1.3308	1.0083	0.0045	0.3225	1.1307e−04	0.164

pfx, pfy, visx, visy are pressure and shear stress forces in the x- and y-direction acting on the cylinder.

Table 6
Data for Case 4

	Lift	Drag	pfx	pfy	visx	visy	Strouhal
Max	0.3264	1.3477	0.9917	0.2882	0.3373	−0.0432	–
Min	−0.3265	1.3291	1.0086	−0.2883	0.3393	−0.0432	–
Mean	0.0085	1.3385	1.0002	0.0077	0.3383	8.6e−04	0.165

pfx, pfy, visx, visy are pressure and shear stress forces in the x- and y-direction acting on the cylinder.

Table 7
Data for Case 5

	Lift	Drag	pfx	pfy	visx	visy	Strouhal
Max	0.3508	1.3838	1.0345	0.3068	0.3495	0.0499	–
Min	−0.3511	1.3588	1.0120	−0.3071	0.3466	−0.0500	–
Mean	−0.0034	1.3714	1.0234	−0.0027	0.3480	−7.1019e−04	0.162

pfx, pfy, visx, visy are pressure and shear stress forces in the x- and y-direction acting on the cylinder.

Table 8
Data for Case 6

	Lift	Drag	pfx	pfy	visx	visy	Strouhal
Max	0.3252	1.3476	1.0047	0.2858	0.3430	0.0443	–
Min	−0.3254	1.3301	0.9889	−0.2859	0.3411	−0.0443	–
Mean	0.0089	1.3389	0.9968	0.0079	0.3421	9.9330e−04	0.165

pfx, pfy, visx, visy are pressure and shear stress forces in the x- and y-direction acting on the cylinder.

Table 9
Data for Case 7

	Lift	Drag	pfx	pfy	visx	visy	Strouhal
Max	0.3268	1.3499	1.0077	0.2878	0.3423	0.0439	–
Min	−0.3268	1.3314	0.9910	−0.2878	0.3403	0.0439	–
Mean	0.0087	1.3406	0.9993	0.0078	0.3413	9.2e−4	0.165

pfx, pfy, visx, visy are pressure and shear stress forces in the x- and y-direction acting on the cylinder.

well with the references. Moreover, we include Case 1 to show the effect the far-field boundary has on the solution. The difference from Case 4 (same order of accuracy and resolution) is not big, which shows that the far-field boundary conditions derived in [19] are good and reasonably transparent.

In Fig. 4, a vector plot of the velocity near a small part of the cylinder surface is shown. Even at this coarse resolution the penalty terms at the boundary forces the velocities to be close to 0. Note also that the direction of the vectors is along the boundary showing that these underresolved boundary conditions tend to act like Euler wall boundary conditions. The extent to which the velocity slips at boundary is proportional to the overall resolution of the calculation. This supports our claim that the slip velocity can be used as a measure of the

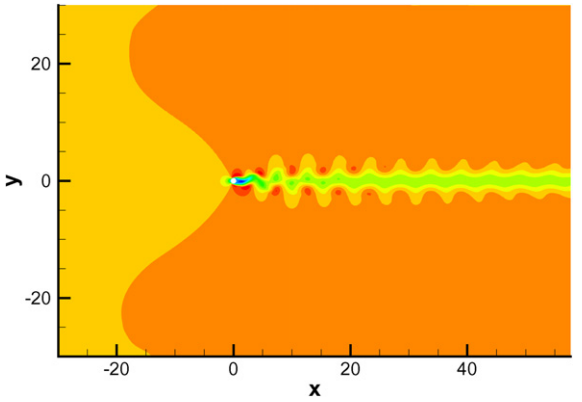

Fig. 5. Plot of ρu in Case 7 at $T = 1500$.

Table 10
Reference data for circular cylinder at $Ma = 0.1$ and $Re = 100$

Average	Pressure drag	Viscous drag	Drag	Strouhal
Kwon and Choi	1.0	0.34	1.34	0.165
	Max drag	Max lift		
Kravchenko et al.	1.286–1.405	0.301–0.3501		0.162–0.167
Williamson	–	–	–	0.161

overall accuracy. Another observation is that, given such underresolved calculations as in Case 4 and Case 2 it is likely that the overall accuracy would be degraded if the no-slip condition was to be enforced exactly, as the rest of the grid does not have a resolution to support that. That leads to the interpretation that the resulting slip velocity can be viewed as part of a boundary layer surrounding a body of slightly different shape. Any body with a shape differing from the cylinder less than the local grid size can be said to be approximated by that particular grid. Hence, we claim that there is no danger in allowing a slip velocity so long as it relates precisely to the resolution. In this case it does.

3.4. Efficiency

We have shown that higher order of accuracy yields smaller errors on a given grid, but the time to compute a solution of a given error is the real measure of efficiency.

To estimate the efficiency, we note that the data of Case 4 are very similar to Case 6. Hence, we should compare run time for the 3rd-order scheme on the fine grid with the 5th-order scheme on the medium grid. The result is shown in Table 11. We run until $T = 1.0$ and measure the time and note that the 5th-order scheme is about three times faster than the 3rd-order. Since we can not know for sure that the two cases have comparable accuracy, an even more unfavorable case for the 5th-order scheme would be to assume that a 2nd-order scheme would perform as well on the fine grid as the 5th-order on the medium grid. We include that test in Table 11 and conclude that even here the 5th-order scheme outperforms the 2nd-order by a factor

Table 11
Run time for three different cases ($T_{\text{final}} = 1.0$)

Order	Time (s)
2 (fine)	58
3 (fine)	90
5 (medium)	27

of two. (We emphasize that we run at the maximum possible CFL in each case.) In 3-D the difference would be even larger in advantage of the 5th-order scheme.

4. Conclusions

We have shown that the no-slip boundary condition together with a boundary condition on the temperature imply well-posedness. The main result of this article is the derivation of a stable numerical procedure for the wall boundary conditions, using SBP-SAT finite difference schemes. A number of different numerical computations for a cylinder in free-stream at $Ma = 0.1$ and $Re = 100$, have been performed that highlight the robustness and accuracy of the penalty imposition of the wall boundary conditions.

The robustness of this technique was demonstrated with the initial behavior of a computation with a free-stream initial data that were incompatible with the boundary data. The computation was perfectly stable and the solution quickly and smoothly adjusted to satisfy the no-slip conditions. We used the deviation from 0 for the discrete solution of u and v at the wall, to show that the errors on the wall are small and that the approximately correct convergence rates were obtained.

Long time calculations and measurement of forces on the cylinder showed good agreement with established results in the literature. Also, increased formal order of accuracy resulted in better results in full agreement with the previous study of the deviation of the no-slip condition at the wall. This observation led us to state (without a proof) that the SAT technique to impose the boundary conditions also supplies us with a tool to measure the accuracy for any discrete solution. That is, the accuracy to which the boundary conditions are satisfied reflects the overall accuracy of the discrete solution.

Finally, a comparison of the 2nd-, 3rd- and 5th-order scheme showed the superior computational efficiency of high-order methods in terms of wall-clock time.

Appendix A. Flow chart for implementation

Below we will summarize the scheme and present a flow chart for the implementation of the wall boundary conditions. For convenience of the reader we repeat (13)

$$(\mathbf{Ju})_t + \mathbf{D}_\xi(\widehat{\mathbf{F}}^{\mathbf{I}} - \epsilon\widehat{\mathbf{F}}^{\mathbf{V}}) + \mathbf{D}_\eta(\widehat{\mathbf{G}}^{\mathbf{I}} - \epsilon\widehat{\mathbf{G}}^{\mathbf{V}}) + \mathbf{D}_\zeta(\widehat{\mathbf{H}}^{\mathbf{I}} - \epsilon\widehat{\mathbf{H}}^{\mathbf{V}}) = \mathbf{0}$$

and the penalty term (19) expressed in the conservative variables.

$$\text{penalty} = \sigma^{\mathrm{I1}}(\mathbf{P}_\xi^{-1}\mathbf{E}_{0\xi}\widehat{\mathbf{A}}_1'(\mathbf{u} - \mathbf{g}^{\mathbf{I1}})) + \epsilon\sigma^{\mathrm{I2}}(\mathbf{P}_\xi^{-1}\mathbf{E}_{0\xi}\widehat{\mathbf{I}}(\mathbf{u} - \mathbf{g}^{\mathbf{I2}})).$$

In a computer code all these relations have to be evaluated at each grid point. We stress that by not using bold face characters below. We will integrate in time using a Runge–Kutta scheme and we pose the scheme as $\mathbf{u}_t = \text{rhs}$ where

$$\begin{aligned}\text{rhs} = \frac{1}{J}(&-D_\xi(\widehat{F}^{\mathrm{I}} - \epsilon\widehat{F}^{\mathrm{V}}) - D_\eta(\widehat{G}^{\mathrm{I}} - \epsilon\widehat{G}^{\mathrm{V}}) - D_\zeta(\widehat{H}^{\mathrm{I}} - \epsilon\widehat{H}^{\mathrm{V}}) + \sigma^{\mathrm{I1}}(P_\xi^{-1}E_{0\xi}\widehat{A}_{1w}'(u - g^{\mathrm{I1}}))\\ &+ \epsilon\sigma^{\mathrm{I2}}(P_\xi^{-1}E_{0\xi}\widehat{I}(w - g_w^{\mathrm{I2}}))).\end{aligned} \tag{38}$$

The penalty term enforces a wall boundary condition at $\xi = 0$ (and will only be non-zero if rhs is evaluated at a boundary point). At any point on the $\xi = 0$ boundary we have $\widehat{A}_1 = X^{\mathrm{T}}\Lambda X$ where $\widehat{A}_1$ is the Jacobian of $\widehat{F}^{\mathrm{I}}$ at that point. $\Lambda = \mathrm{diag}(u_n, u_n, u_n, u_n + a, u_n - a)$. The transformation matrix X can be found in [17]. (Note that the transformation takes the conservative variables directly to the characteristic variables.) The other five sides in the 3D computational box will have the corresponding penalty terms.

In each grid block, the solution is stored in a multi-index variable $\mathbf{u}$. At each of the six sides we need three variables u^B, $g^{\mathrm{I1}}, g^{\mathrm{I2}}$, $i = 1, \ldots, 6$ of the size of the corresponding side (that is a plane in 3D and a line in 2D). We initialize by giving $\mathbf{u}$ values and copy the boundary values of $\mathbf{u}$ into u^B at each side. We construct and store the boundary values to be used for the inviscid penalty term in g^{I1}, and in case of a wall the no-slip values and temperature value is put in g^{I2}. To construct the data we use the boundary values u^B extract the variables that are not to be given a value and use them along with the given boundary data to construct $g^{I1,I2}$.

Example 1. Assume a wall at $\xi = 0$. Then $u = v = w = 0$, $T = T_{\text{wall}}$ and u^B is the solution at $\xi = 0$. Using u^B we can compute the local value of ρ. Then we construct (on conservative form) $g^{\text{I2}} = (\rho, 0, 0, 0, \frac{\rho T_{\text{wall}}}{\gamma(\gamma-1)})^{\text{T}}$ at each point on the side.

The values on the penalty parameters, σ^{I1} and σ^{I2} are given by Lemma 2.2 and Theorem 2.3.

Next, we present the flow in the code. Loop over time and Runge–Kutta stages and compute the following at each stage:

1. Form inviscid and viscous fluxes.
2. Compute difference approximations of all the fluxes.
3. Loop *: Loop over all sides, i. If the side, i, is a wall, loop over all points at that side.
   (a) Compute Roe-average between u^B and g^{I1}. (Denote the result u_{roe}.)
   (b) Compute $X(u_{\text{roe}})$ and $\Lambda'(u_{\text{roe}})$, which is the diagonal matrix with non-zero entries corresponding to the ingoing characteristics.
   (c) Compute $A' = X^{\text{T}}\Lambda' X$.
   (d) Compute penalty$^i = \sigma^{\text{I1}} A'(u^B - g^{\text{I1}}) + \sigma^{\text{I2}} I(u^B - g^{\text{I2}})$.
   (e) Scale penalty: penalty$^i := (P_Y^{-1}/J) \cdot$ penalty^i. ($Y = \xi, \eta, \zeta$ depending on the direction of the normal on the side.)
4. Add penalty^i to rhs at the points corresponding to side i.
5. End loop *.
6. Use rhs in the Runge–Kutta stage.

Remark. The same routine can be used for all boundaries. X and Λ' will depend on the normal direction and will automatically be correct whichever boundary we consider. Care is only needed in the choice of ingoing characteristics and the sign of the final penalty term.

Remark. It is straightforward to include the treatment of far-field boundaries and grid–block interfaces in the above procedure. We need to add an extra penalty term for the viscous flux and add an additional data variable, g^{V}, to be used in that penalty term.

If the side is a far-field boundary $\sigma^{\text{I2}} = 0$. We also include the possibility of time dependent data, i.e. g^{I1} is updated at each stage.

If the side is an interface we would need to communicate u^B and the viscous fluxes in the above procedure. We would use the above penalty terms and the extra penalty on the viscous flux. $g^{\text{I1}} = g^{\text{I2}} = u^{B2}$ and $g^{\text{V}} = F^{B2}$, where u^{B2} and F^{V2} is the data obtained from the connecting block. The penalty parameter σ^{I2} would be slightly different and depend on the P matrices on both sides of the interface, but would still be $\sim 1/h$ as in the present article. (A thorough derivation is the subject of a future article.)

References

[1] Saul Abarbanel, David Gottlieb, Optimal time splitting for two- and three-dimensional Navier–Stokes equations with mixed derivatives, J. Comput. Phys. (1981).
[2] M.H. Carpenter, D. Gottlieb, S. Abarbanel, Time-stable boundary conditions for finite-difference schemes solving hyperbolic systems: methodology and application to high-order compact schemes, J. Comput. Phys. 111 (2) (1994).
[3] M.H. Carpenter, J. Nordström, D. Gottlieb, A stable and conservative interface treatment of arbitrary spatial accuracy, J. Comput. Phys. 148 (1999).
[4] B. Gustafsson, H.-O. Kreiss, J. Oliger, Time Dependent Problems and Difference Methods, John Wiley & Sons, 1995.
[5] R.A. Horn, C.R. Johnson, Matrix Analysis, Cambridge University Press, 1990.
[6] Kiyoung Kwon, Haecheon Choi, Control of laminar vortex shedding behind a circular cylinder using splitter plates, Phys. Fluids 8 (2) (1996) 479–486.
[7] Heinz-Otto Kreiss, Jens Lorenz, Initial Boundary Value Problems and the Navier–Stokes Equations, Academic Press, New York, 1989.

[8] A.G. Kravchenko, P. Moin, K. Shariff, B-spline method and zonal grids for simulations of complex turbulent flows, J. Comput. Phys. 151 (1999) 757–789.
[9] H.-O. Kreiss, G. Scherer, Finite element and finite difference methods for hyperbolic partial differential equations, Mathematical Aspects of Finite Elements in Partial Differential Equations, Academic Press, 1974.
[10] H.-O. Kreiss, G. Scherer, On the existence of energy estimates for difference approximations for hyperbolic systems, Technical report, Department of Scientific Computing, Uppsala University, 1977.
[11] K. Mattsson, M. Svärd, M.H. Carpenter, J. Nordström, High-order accurate computations for unsteady aerodynamics, Comput. Fluids 36 (3) (2007) 636–649.
[12] Ken Mattsson, Jan Nordström, Summation by parts operators for finite difference approximations of second derivatives, J. Comput. Phys. 199 (2) (2004).
[13] Ken Mattsson, Magnus Svärd, Jan Nordström, Stable and accurate artificial dissipation, J. Sci. Comput. 21 (1) (2004) 57–79.
[14] J. Nordström, M.H. Carpenter, Boundary and interface conditions for high-order finite-difference methods applied to the Euler and Navier–Stokes equations, J. Comput. Phys. 148 (1999).
[15] J. Nordström, M.H. Carpenter, High-order finite difference methods, multidimensional linear problems, and curvilinear coordinates, J. Comput. Phys. 173 (2001).
[16] Jan Nordström, Magnus Svärd, Well posed boundary conditions for the Navier–Stokes equations, SIAM J. Numer. Anal. 43 (3) (2005) 1231–1255.
[17] T.H. Pulliam, D.S. Chaussee, A diagonal form of an implicit approximate-factorization algorithm, J. Comput. Phys. 39 (1981) 347–363.
[18] P.L. Roe, Approximate riemann solvers, parameter vectors and difference schemes, J. Comput. Phys. 43 (1981) 357–372.
[19] M. Svärd, M.H. Carpenter, J. Nordström, A stable high-order finite difference scheme for the compressible Navier–Stokes equations, far-field boundary conditions, J. Comput. Phys. 225 (1) (2007) 1020–1038.
[20] Magnus Svärd, Ken Mattsson, Jan Nordström, Steady state computations using summation-by-parts operators, J. Sci. Comput. 24 (1) (2005) 79–95.
[21] Magnus Svärd, Jan Nordström, On the order of accuracy for difference approximations of initial-boundary value problems, J. Comput. Phys. 218 (1) (2006) 333–352.
[22] Bo Strand, Summation by parts for finite difference approximations for d/dx, J. Comput. Phys. 110 (1994).
[23] Magnus Svärd, On coordinate transformation for summation-by-parts operators, J. Sci. Comput. 20 (1) (2004).
[24] C.H.K. Williamson, Defining a universal and continuous Strouhal–Reynolds number relationship for the laminar vortex shedding of a circular cylinder, Phys. Fluids 31 (10) (1988) 2742–2744.